Tropospheric tomography – integration of ground- and space-based GNSS observations

Natalia Hanna[1], Robert Weber[1]

[1]Department of Geodesy and Geoinformation, TU Wien, Vienna, Austria

ABSTRACT

On the way transmitter-receiver, the Global Navigation Satellite Systems (GNSS) signal is attenuated and delayed by the presence of water vapor. This information serves as the input to the GNSS tomography - a robust technique in water vapor estimation concerning its amount and distribution in the troposphere. GNSS rays pass through the tomographic grid built over a dense network of ground-based GNSS stations. Due to the constant movement of the GNSS satellites influencing their elevation angle and visibility, the measurement geometry varies in time. The model elements are either over or under-determined during the chosen time span within the area of interest; hence, the system of observation equations is mixed-determined.

However, to enhance the tomographic solution, the model can be supplied with additional data, e.g., from the radio occultation (RO). The RO technique provides the space-based signal delay between the low Earth orbit (LEO) and GNSS satellites. Products obtained from the RO measurements consist of bending angles and vertical dry- and wet-atmosphere data.

In this study, we analyze the COSMIC-1 radio occultation events in the tomographic domain located in the Netherlands in February 2018. The observation system in the ATom GNSS software was extended with the space-based wet refractivity profiles (level 2 data).

1. GNSS ground- and space based tomography principles

GNSS troposphere tomography obtains a **3-D field of wet refractivity** in the lower atmosphere (up to ~10 km), based on the GNSS signal delays. For space observations (Fig. 1), the angle through which the ray is deflected – the bending angle α – is a function of the impact parameter a, determined from the measured Doppler frequency shift or phase delay of the received signal. For ground observations (Fig. 2), Slant Wet Delay (SWD) can be modeled as an integral of the wet refractivity (N_w) along the ray path. The inversion of a set of equations leads to the estimation of the wet refractivity distribution.

1.1. Space-based observations

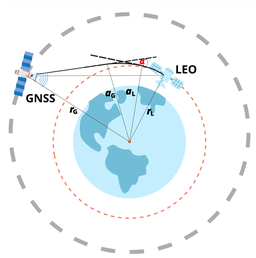

After the ionospheric affects have been removed, the bending angle is converted to the refractive index n(r) using the Abel integral algorithm under the assumption of local spherical symmetry:

$$n(r) = \exp\left[\frac{1}{\pi}\int_x^\infty \frac{\alpha(a)}{\sqrt{a^2 - x^2}}\,\mathrm{d}a\right]$$

The refractvity N used to generate the so-called dry and wet atmospheric profiles is then calculated:

$$\mathrm{N}(r) = (n-1)\times 10^6$$

Figure 1. The geometry of a radio occultation measurement showing the refracted ray from a transmitting satellite (on the left) to a receiving satellite (on the right).

1.2. Ground-based observations

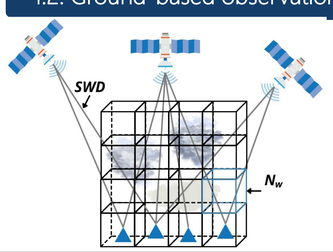

$$SWD = 10^{-6}\int_s N_w(s)\mathrm{d}s$$

Figure 2. Scheme of GNSS rays in the tomographic domain.

1.3. System of equations

Ground-based solution

$$\overline{SWD} = A \cdot \overline{N_w}$$

observed | Jacobi matrix | estimated

$$\overline{SWD} = \begin{bmatrix} SWD_1 \\ SWD_2 \\ \vdots \\ SWD_l \end{bmatrix} \quad A = \begin{bmatrix} \frac{\partial SWD_1}{\partial N_{w1}} & \frac{\partial SWD_1}{\partial N_{w2}} & \cdots & \frac{\partial SWD_1}{\partial N_{wm}} \\ \frac{\partial SWD_2}{\partial N_{w1}} & \frac{\partial SWD_2}{\partial N_{w2}} & \cdots & \frac{\partial SWD_2}{\partial N_{wm}} \\ \vdots & \vdots & \ddots & \vdots \\ \frac{\partial SWD_l}{\partial N_{w1}} & \frac{\partial SWD_l}{\partial N_{w2}} & \cdots & \frac{\partial SWD_l}{\partial N_{wm}} \end{bmatrix} \quad \overline{N_w} = \begin{bmatrix} N_{w1} \\ N_{w2} \\ \vdots \\ N_{wm} \end{bmatrix}$$

Combined solution

$$SWD_{\mathrm{ext}} = \begin{bmatrix} SWD \\ N_{\mathrm{apr}} \\ N_{w\mathrm{RO}} \end{bmatrix} \quad \mathbf{A}_{\mathrm{ext}} = \begin{bmatrix} \mathbf{A} \\ \mathbf{A}_{\mathrm{apr}} \\ \mathbf{A}_{\mathrm{RO}} \end{bmatrix} \quad P_{\mathrm{ext}} = \begin{bmatrix} P \\ P_{\mathrm{apr}} \\ P_{\mathrm{RO}} \end{bmatrix}$$

1.4. Tomographic solution – inversion

$$\overline{N_w} = \mathrm{inv}(\mathbf{A}) \cdot \overline{SWD}$$

The estimated 3-D fields of wet refractivity depend on humidity in the troposphere, thus they have a great potential to serve as a source of data for the **weather prediction models**.

2. Integrated tomographic solution

The tomography solution over the network of 24 ground-based GNSS stations (Fig. 3) was calculated. In February 2018 five RO events were located in the tomographic domain. The differences in wet refractivity fields between the combined and ground-based tomographic solution for DOY 033.2018 at 02 UTC are shown.

2.1. Tomographic domain

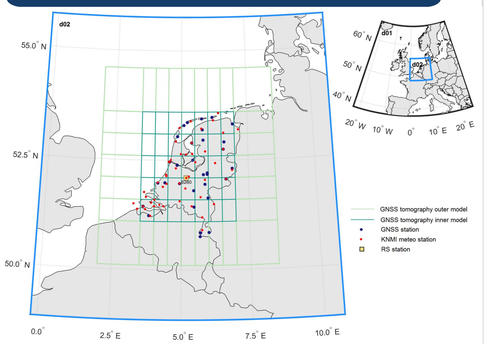

Figure 3. Tomographic domain location.

2.2. Observation weights

$$\sigma SWD_{\mathrm{i}} = \frac{1}{\sin^2 e_{\mathrm{i}}} \cdot \sigma ZTD_{\mathrm{i}}$$

where $\sigma ZTD = 1.5$ mm is based on the post-fit residuals analysis.

Table 1. Wet refractivity uncertainty (COSMIC level2 wetPrf).

Height [km]	Average formal [ppm] (CS1)	Height [km]	vs RS [%] (CS2)
< 1.0	±1	≤ 3.0	±4
1.0 – 4.0	±1	3.1 – 5.0	±2
4.1 – 8.0	±2	5.1 – 10.0	±1
8.0 >	±0.03	10.1 ≥	±1.5

2.3. Wet refractivity field differences

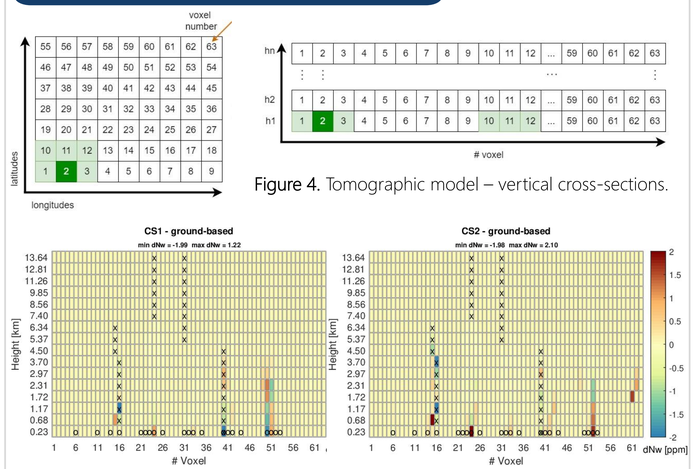

Figure 4. Tomographic model – vertical cross-sections.

Figure 5. Wet refractivity fields differences between the tomographic combined (left-hand panel CS1 and right-hand panel CS2 weights applied) and ground-based solution. The location of RO profiles is depicted by *x*, and GNSS stations location by *o*.

2.4. Weather sites validation

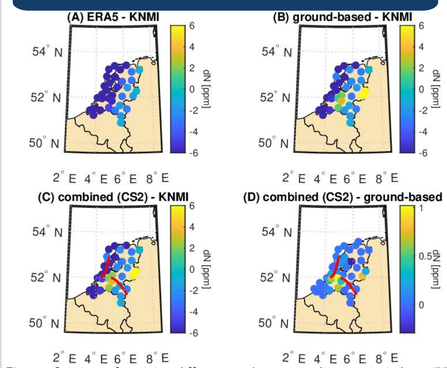

Figure 6. Wet refractivity differences between the a priori data (ERA5), ground-based tomographic solution, combined tomographic solution (CS2), and reference *Nw* values for the network of 50 KNMI stations at the station height. Red lines indicate the location of RO profiles.

3. Conclusions and outlook

Due to the integration of the GNSS ground- and space-based observations, differences in the wet refractivity values (up to 2 ppm) in the voxels located in the vicinity of traversed voxels are obtained.

The combination of the GNSS ground- and space-based observations causes a reduction of wet refractivities in particular voxels, when compared to the ERA5-derived data (negative bias is observed).

Compared to RS data, the differences between the combined and ground-based only tomographic solutions are very small (reduction of RMS ~0.1 ppm; not shown), whereas, in the case of weather sites, the differences reach ~1 ppm. At the surface level, the combined and space-based solutions reduce the root mean square error of wet refractivity by ~1 ppm compared to the ERA5-derived data.

To evaluate the impact of observations integration on meteorological parameters, tomographic wet refractivity assimilation into the Numerical Weather Model will be performed.